

Description of quadrupole collectivity in $N \approx 20$ nuclei with techniques beyond the mean field.

R.R. Rodríguez-Guzmán, J.L. Egido and L.M. Robledo

*Departamento de Física Teórica C-XI, Universidad Autónoma de Madrid,
28049-Madrid, Spain.*

Abstract

Properties of the ground and several collective excited states of the light nuclei $^{30,32,34}Mg$ are described in the framework of the angular momentum projected Generator Coordinate Method using the quadrupole moment as collective coordinate and the Gogny force as the effective interaction. The calculated excitation energies and $B(E2)$ transition probabilities agree reasonably well with experiment. The results clearly indicate that both the restoration of the rotational symmetry and the quadrupole dynamics are key ingredients for the description of the properties of the above mentioned nuclei.

Key words:

PACS: 21.60.Jz, 21.60.-n, 21.10.Re, 21.10.Ky, 21.10.Dr, 27.30.+t

Nowadays, the region of neutron-rich nuclei around $N = 20$ is the subject of active research both in the experimental and theoretical side. The reason is the strong experimental evidence towards the existence of quadrupole deformed ground states in this region. Deformation implies extra binding energy extending thereby the neutron drip line in this region far beyond what could be expected from spherical ground states. On the other hand, the existence of deformed ground states implies that $N = 20$ is not a magic number for the nuclei considered, opening up the possibility for a better understanding of the mechanisms behind the shell structure in atomic nuclei. Among the available experimental data, the most convincing evidence for a deformed ground state is found in the ^{32}Mg nucleus where both the excitation energy of the 2^+ state [1] and the $B(E2, 0^+ \rightarrow 2^+)$ transition probability [2] have been measured. Both quantities are fairly compatible with the expectations for a rotational state. Theoretically, from a shell model point of view, the deformed ground states are a consequence of the lower energies of some intruder $2p - 2h$ neutron excitations into the fp shell as compared to the pure sd configuration [3]. In terms of the mean field picture of the nucleus, a quadrupole deformed ground

state only appears after taking into account the zero point rotational energy correction to the mean field energy [4–8].

In a previous paper [9] we have computed angular momentum projected (AMP) energy landscapes, as a function of the mass quadrupole moment, for the nuclei $^{30-34}Mg$ and $^{32-38}Si$. We have found that the projection substantially changes the conclusions extracted from a pure mean field calculation. In all the nuclei considered, exception made of ^{34}Mg , two coexistent configurations (prolate and oblate) were found with comparable energy indicating thereby that configuration mixing of states with different quadrupole intrinsic deformation had to be considered. The purpose of this paper is to study the effect of such configuration mixing for the nuclei $^{30-34}Mg$. The Si isotopes have been disregarded in this work as there are indications [7] that triaxiality effects could be relevant for the description of their ground states and, for the moment, our calculations are restricted to axially symmetric ($K = 0$) configurations. In our calculations we have used the Gogny force [10] (with the D1S parameterization [11]) which is known to provide reasonable results for many nuclear properties like ground state deformations, moments of inertia, fission barrier parameters, etc, all over the periodic table. As the results presented in this paper will show, this force is also suited for the description of quadrupole collectivity in $N \approx 20$ nuclei. Similar calculations to the ones discussed here using the Skyrme interaction have recently been reported [12].

We have used the angular momentum projected Generator Coordinate Method (GCM) to compute the properties of the ground and several collective excited states of those nuclei. To this end, we have used the following ansatz for the $K = 0$ wave functions of the system

$$|\Phi_\sigma^I\rangle = \int dq_{20} f_\sigma^I(q_{20}) \hat{P}_{00}^I |\varphi(q_{20})\rangle$$

In this expression $|\varphi(q_{20})\rangle$ is the set of axially symmetric (i.e. $K = 0$) Hartree-Fock-Bogoliubov (HFB) wave functions generated by constraining the mass quadrupole moment to the desired values q_{20} , the operator $\hat{P}_{00}^I = \frac{2I+1}{8\pi^2} \int d\Omega d_{00}^I(\beta) e^{-i\alpha J_z} e^{-i\beta J_y} e^{-i\gamma J_z}$ is the usual angular momentum projector with the $K = 0$ restriction [13] and $f_\sigma^I(q_{20})$ are the “collective wave functions” solution of the Hill-Wheeler (HW) equation

$$\int dq_{20} \mathcal{H}^I(q_{20}, \dot{q}_{20}) f_\sigma^I(\dot{q}_{20}) = E_\sigma^I \int dq_{20} \mathcal{N}^I(q_{20}, \dot{q}_{20}) f_\sigma^I(\dot{q}_{20}).$$

In the equation above we have introduced the projected norm $\mathcal{N}^I(q_{20}, \dot{q}_{20}) = \langle \varphi(q_{20}) | \hat{P}_{00}^I | \varphi(q_{20}) \rangle$, and the projected hamiltonian kernel $\mathcal{H}^I(q_{20}, \dot{q}_{20}) = \langle \varphi(q_{20}) | \hat{H} \hat{P}_{00}^I | \varphi(q_{20}) \rangle$. The solution of the HW equation for each value of the angular momentum I determines not only the ground state ($\sigma = 1$), which corresponds to the Yrast

band, but also excited states ($\sigma = 2, 3, \dots$). In order to account for the fact that the mean value of the particle operator $\langle \Phi_\sigma^I | \hat{N}_\tau | \Phi_\sigma^I \rangle$ ($\tau = \pi, \nu$) usually differs from the proton and neutron number we have followed the usual recipe [14,15] of replacing the hamiltonian by $\hat{H} - \lambda_\pi(\hat{N}_\pi - Z) - \lambda_\nu(\hat{N}_\nu - N)$ where λ_π and λ_ν are chemical potentials for protons and neutrons respectively. The intrinsic wave functions have been expanded in a Harmonic Oscillator (HO) basis containing 10 major shells and with equal oscillator lengths to make it closed under rotations [16]. The rotation operator in the HO basis has been computed using the formulas of [17].

Concerning the density dependent part of the Gogny force we have used the usual prescription already discussed in Refs. [15,9,18]. It amounts to use the density

$$\rho(\vec{r}) = \frac{\langle \varphi(q_{20}) | \hat{\rho} e^{-i\beta \hat{J}_y} | \varphi(q_{20}) \rangle}{\langle \varphi(q_{20}) | e^{-i\beta \hat{J}_y} | \varphi(q_{20}) \rangle}$$

in the density dependent part of the interaction when the evaluation of $\langle \varphi(q_{20}) | \hat{H} e^{-i\beta \hat{J}_y} | \varphi(q_{20}) \rangle$ is required in the calculation of the projected hamiltonian kernels.

As the generating states $\hat{P}_{00}^I | \varphi(q_{20}) \rangle$ are not orthogonal, the “collective amplitudes” $f_\sigma^I(q_{20})$ cannot be easily interpreted. This drawback can be easily overcome by introducing [19] the so-called “natural” states $|k^I\rangle = (n_k^I)^{-1/2} \int dq_{20} u_k^I(q_{20}) | \varphi(q_{20}) \rangle$ which are defined in terms of the eigenstates $u_k^I(q_{20})$ and eigenvalues n_k^I of the projected norm, i.e. $\int dq_{20} \mathcal{N}^I(q_{20}, q_{20}) u_k^I(q_{20}) = n_k^I u_k^I(q_{20})$. The correlated wave functions $|\Phi_\sigma^I\rangle$ are written in terms of the natural states as $|\Phi_\sigma^I\rangle = \sum_k g_k^{\sigma, I} |k^I\rangle$ where the new amplitudes $g_k^{\sigma, I}$ have been introduced. Finally, in order to express the amplitudes $g_k^{\sigma, I}$ as a function of q_{20} the collective wave functions $g_\sigma^I(q_{20}) = \sum_k g_k^{\sigma, I} u_k(q_{20})$ are defined. They are orthogonal and therefore their module squared has the meaning of a probability. The introduction of the natural states also reveals a particularity of the HW equation: if the norm has eigenvalues with zero value they have to be removed for a proper definition of the natural states (i.e. linearly dependent states are removed from the basis). In practical cases, in addition to the zero value eigenvalues also the eigenvalues smaller than a given threshold have to be removed to ensure the numerical stability of the solutions of the HW equation.

In figure 1 we have plotted the $I = 0\hbar, 2\hbar, 4\hbar, 6\hbar$ and $I = 8\hbar$ projected energies as a function of q_{20} for the nuclei $^{30,32,34}Mg$. The HFB energies have also been plotted for comparison. The projected energy curves can be regarded as the potential energies felt by the quadrupole collective motion and therefore give us indications of where the collective wave functions will be concentrated. Before commenting the physical contents of the curves we have to mention that, except for the $I = 0\hbar$ curves, several values around $q_{20} = 0$ are omitted.

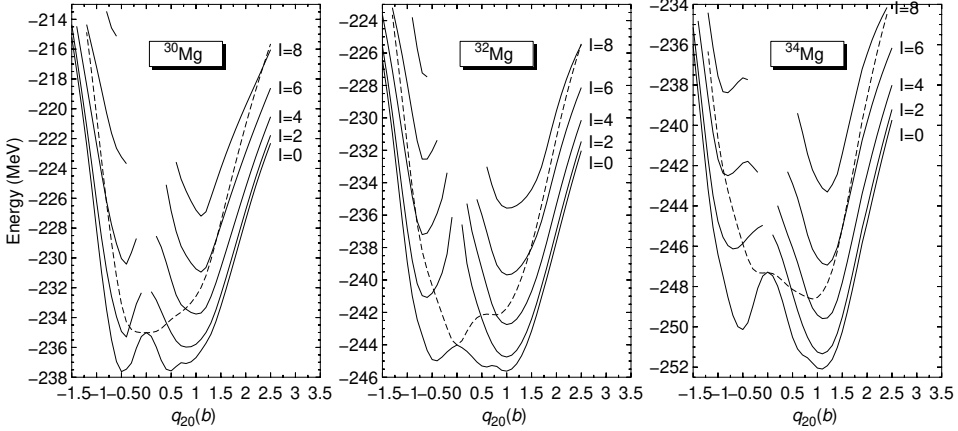


Fig. 1. The HFB (dashed line) and angular momentum projected energies ($I = 0\hbar, 2\hbar, \dots, 8\hbar$) for the nuclei considered. See text for further comments.

They correspond to intrinsic configurations with a very small value of the norm $\mathcal{N}^I(q_{20}, q_{20})$, that is, to configurations whose $I = 2\hbar, 4\hbar, \dots$ contents are very small. As a consequence, the evaluation of the projected energies in these cases is vulnerable to strong numerical inaccuracies. Fortunately, the smallness of their projected norms guarantees that these configurations do not play a role in the configuration mixing calculation (the associated norm eigenvalues n_k^I are very small) and therefore can be safely omitted.

Coming back to the projected energy surfaces, we observe that for $I = 0\hbar$ and $2\hbar$ a prolate and an oblate minima appear with almost the same energy for the nucleus ^{30}Mg whereas the prolate minimum becomes deeper than the oblate one for $^{32,34}Mg$. For increasing spins either the prolate minimum becomes significantly deeper than the oblate one or the oblate minimum is washed out. The prolate minima are located, for all nuclei and spin values, around $q_{20} = 1b$ that corresponds to a β deformation parameter of 0.4. On the other hand, the HFB energy curves show a behavior rather different from the $I = 0\hbar$ projected curves and show a spherical minimum for $^{30,32}Mg$ and a prolate one for ^{34}Mg .

It is interesting to consider the spherical orbit occupancy of the intrinsic wave functions by computing the quantity $\nu(nlj) = \langle \varphi(q_{20}) | \sum_m c_{nljm}^+ c_{nljm} | \varphi(q_{20}) \rangle$ where c_{nljm} are the annihilation operators corresponding to spherical harmonic oscillator wave functions. In the nucleus ^{32}Mg the neutron $\nu(1f_{7/2})$ occupancy is zero for $q_{20} = 0$ whereas it is almost 2 at the minimum of the projected energy (i.e. $q_{20} = 1b$). The conclusion is clear, the zero point energy associated to the restoration of the rotational symmetry favors the configuration in which a couple of neutrons have been promoted from the sd shell to the $f_{7/2}$ shell. This is in good agreement with the Shell Model picture of deformation in these nuclei [?,3].

In figure 2 the collective wave functions squared $|g_\sigma^I(q_{20})|^2$ for the two lowest

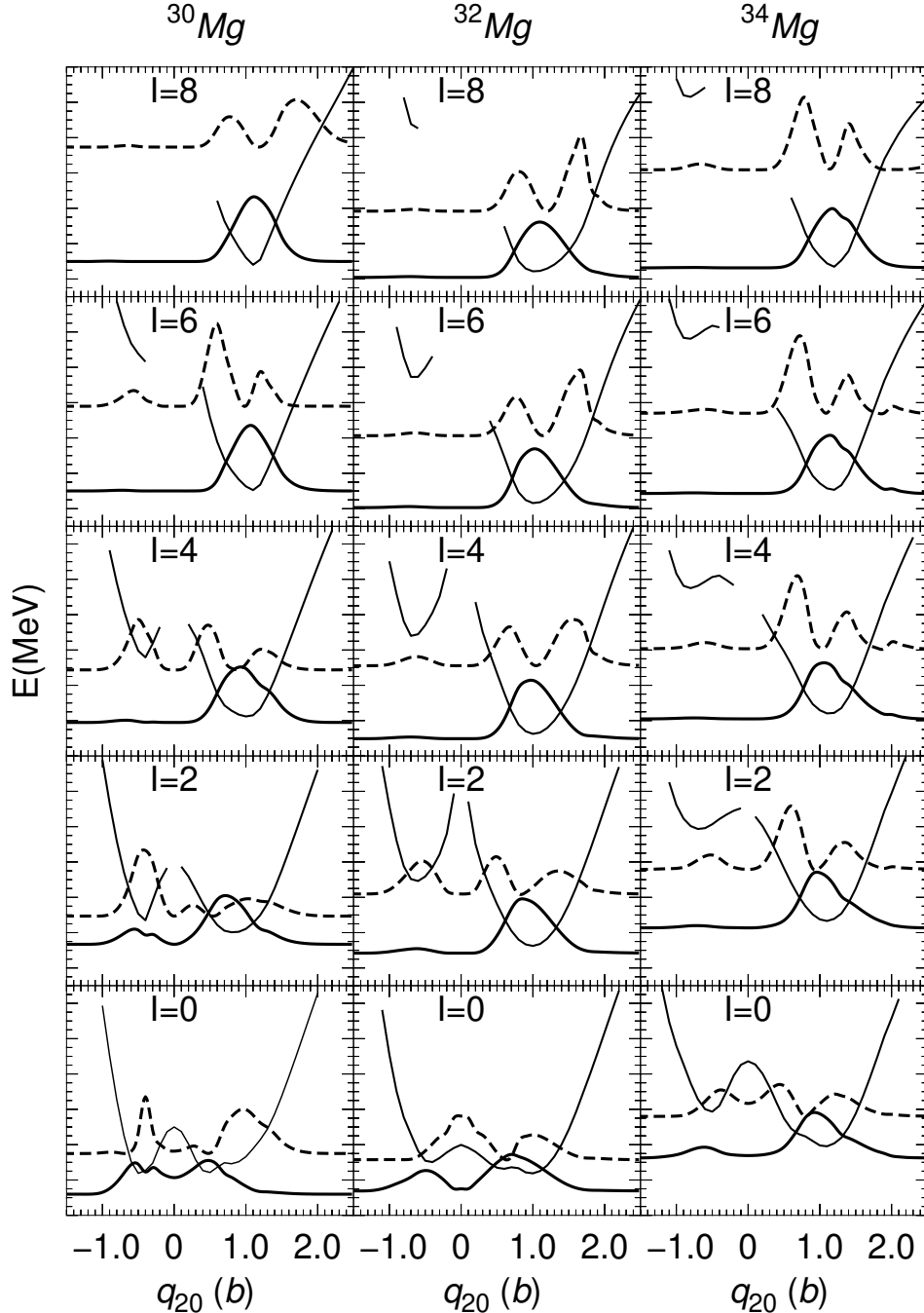


Fig. 2. The collective amplitudes $|g_\sigma^I(q_{20})|^2$ (thick lines) for $\sigma = 1$ (full) and 2 (dashed) and spin values of $I = 0\hbar, \dots, 8\hbar$ for the nuclei ^{30}Mg , ^{32}Mg and ^{34}Mg . The projected energy curve for each spin is also plotted (thin line). The y-axis scales are in energy units and always span an energy interval of 13 MeV (minor ticks are 0.5 MeV apart). The collective wave functions $|g_\sigma^I(q_{20})|^2$ have also been plotted against the energy scale after a proper scaling and shifting, that is, the quantity $E_\sigma^I + 15 \times |g_\sigma^I(q_{20})|^2$ is the one actually plotted. With this choice of scales we can read from the figure the energy gain due to the quadrupole fluctuations by considering the position of the wave functions' tail relative to the projected curve.

	^{30}Mg				^{32}Mg				^{34}Mg			
I	$(\bar{q}_{20})_1^I$	Σ_1^I	$(\bar{q}_{20})_2^I$	Σ_2^I	$(\bar{q}_{20})_1^I$	Σ_1^I	$(\bar{q}_{20})_2^I$	Σ_2^I	$(\bar{q}_{20})_1^I$	Σ_1^I	$(\bar{q}_{20})_2^I$	Σ_2^I
0	0.091	0.558	0.626	0.685	0.436	0.692	0.396	0.601	0.788	0.691	0.440	0.723
2	0.579	0.588	0.092	0.750	0.885	0.482	0.393	0.859	1.052	0.455	0.644	0.658
4	0.962	0.387	0.215	0.716	1.012	0.388	1.041	0.723	1.136	0.387	0.819	0.573
6	1.087	0.300	0.581	0.557	1.084	0.363	1.264	0.554	1.188	0.354	0.860	0.528
8	1.131	0.289	1.470	0.562	1.151	0.368	1.293	0.515	1.226	0.332	0.926	0.560

Table 1

The average intrinsic quadrupole moment $(\bar{q}_{20})_\sigma^I$ and fluctuations $\Sigma_\sigma^I = \sqrt{(\bar{q}_{20}^2)_\sigma^I}$ in barns for the three nuclei considered.

solutions $\sigma = 1$ and 2 obtained in the AMP-GCM calculations are depicted. We also show in each panel the projected energy for the corresponding spin. We observe that the 0_1^+ ground state wave functions of the ^{30}Mg and ^{32}Mg nuclei contain significant admixtures of the prolate and oblate configurations whereas for ^{34}Mg the wave function is almost completely located inside the prolate minimum. At higher spins, however, the ground state wave functions are located inside the prolate minimum in all the nuclei studied. Concerning the first excited states ($\sigma = 2$) we notice that in the nucleus ^{34}Mg for spins higher than zero the collective wave functions show a behavior reminiscent of a β vibrational band: they are located inside the prolate minimum and have a node at a q_{20} value near the point where the ground state collective wave functions attain their maximum values. Contrary to the case of a pure β band, the collective wave functions of fig. 2 are not symmetric around the node and therefore can not be considered as harmonic vibrations. On the other hand, the 0_2^+ state of ^{34}Mg is an admixture of prolate and oblate configurations and can not be considered as a β vibrational state. The same pattern is also seen in the other two nuclei but with slight differences: the β like bands appear at spins 4 and 6 for ^{32}Mg and ^{30}Mg respectively. It is also worth pointing out that from the position of the tails of the collective wave functions relative to the projected energies (see figure caption) we can read the energy gain due to the quadrupole fluctuations. The energy gain is maximal at $I = 0\hbar$ (0.9, 1 and 0.7 MeV for ^{30}Mg , ^{32}Mg and ^{34}Mg respectively) and quickly decreases with spin reflecting the narrowing of the projected minima with spin.

In order to understand in a more quantitative way the collective wave functions just discussed it is convenient to analyze the average $(\bar{q}_{20})_\sigma^I = \int dq_{20} |g_\sigma^I(q_{20})|^2 q_{20}$, that gives us a measure of the deformation of the underlying intrinsic states, and $(\bar{q}_{20}^2)_\sigma^I = \int dq_{20} |g_\sigma^I(q_{20})|^2 q_{20}^2 - ((\bar{q}_{20})_\sigma^I)^2$ that serves as an estimation of the wave functions' spreading. The values of $(\bar{q}_{20})_\sigma^I$ and $\Sigma_\sigma^I = ((\bar{q}_{20}^2)_\sigma^I)^{1/2}$ corresponding to the collective wave functions of figure 2 are given in table I. We observe that the 0_1^+ and 2_2^+ states of ^{30}Mg are spherical (but with strong

	Calc. Energies(MeV)			Exp.	Calc. $B(E2)e^2 fm^4$			Exp.
	$0_1^+ - 2_1^+$	$0_1^+ - 0_2^+$	$2_1^+ - 2_2^+$		$0_1^+ - 2_1^+$	$0_1^+ \rightarrow 2_1^+$	$0_1^+ \rightarrow 2_2^+$	
^{30}Mg	2.15	2.30	1.60	1.482	229	3	218	300(*)
^{32}Mg	1.46	1.77	3.35	0.885	395	3.4	199	454 ± 78
^{34}Mg	1.02	2.35	3.31	0.75(*)	525	0	290	580(*)

Table 2

Calculated and experimental results for excitation energies and $B(E2, 0_{\sigma_1}^+ \rightarrow 2_{\sigma_2}^+)$ transition probabilities. In the experimental data columns values marked with an (*) correspond to Monte Carlo Shell Model results taken from Ref. [20]. The experimental data for the excitation energies have been taken from [1] for the ^{32}Mg nucleus and from [23] for ^{30}Mg . The $B(E2)$ transition probability has been taken from [2].

fluctuations in the q_{20} degree of freedom) whereas the 2_1^+ state is deformed ($\beta = 0.25$). On the other hand, the 0_1^+ states of ^{32}Mg and ^{34}Mg are deformed with β values of 0.16 and 0.3 respectively and have a Σ_1^I value rather high, possibly due to the small oblate hump. For spins higher than $I = 0\hbar$ in $^{32,34}Mg$ and $I = 4\hbar$ in ^{30}Mg the ground state band is strongly deformed. The spreading of the wave functions gets smaller for increasing spins as expected. The excited bands also get more deformed for increasing spin, but their β values never coincide with that of the ground state band. Obviously, their spreadings are bigger than for the ground state band.

In table 2 the energy splittings between different states and the $E2$ transition probabilities among them are compared with the available experimental data. Concerning the $B(E2, 0_1^+ \rightarrow 2_1^+)$ transition probabilities we find a very good agreement with the only known experimental value and with the theoretical predictions of Utsumo et al. [20] using the Monte Carlo Shell Model (MCSM). The 2_1^+ excitation energies rather nicely follow the isotopic trend but they are larger than the experimental values by a factor of roughly 1.5. This discrepancy could be the result of using angular momentum projection after variation (AMPAV) instead of the more complete projection before variation (AMPBV) that will require for each value of the angular momentum the calculation of the generating states from the variational principle on the projected energy. Usually, the AMPBV method yields to rotational bands with moments of inertia larger than the AMPAV ones [14,21].

A full AMPBV is, unfortunately, extremely costly to implement with large configuration spaces. Therefore, to estimate the effect of AMPBV in our results, one has to resort to the selfconsistent cranking method which is an approximation to AMPBV in the limit of large deformations. We have chosen the intrinsic state with $q_{20} = 1b$ as the most representative configuration (it approximately corresponds to the prolate minima in all the nuclei considered

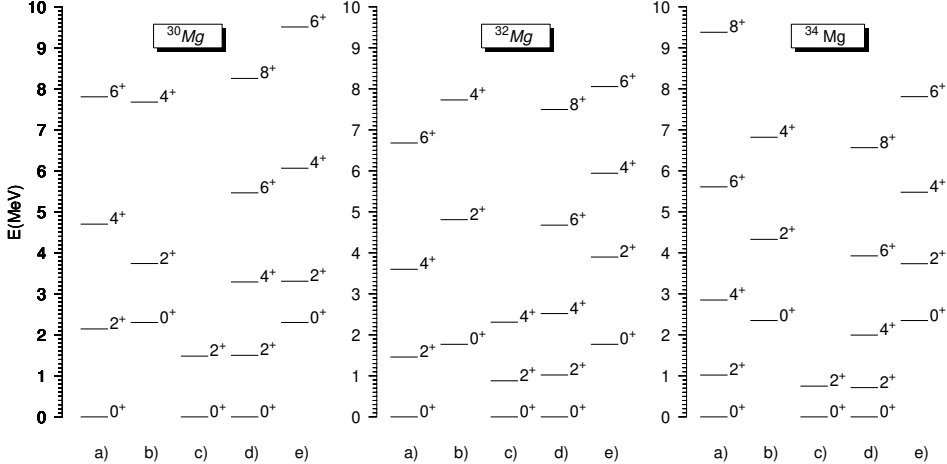


Fig. 3. Collective bands for the three nuclei studied. Bands a) and b) correspond to the GCM results for the ground and first excited band. c) is the experimental band (in the case of ^{34}Mg the MCSM prediction of [20] has been used). Finally, bands d) and e) are the GCM results quenched by the factor 0.7 discussed in the text.

) and computed the projected energies. In addition, selfconsistent cranking calculations with the constraints $q_{20} = 1b$ in the quadrupole moment and $\langle J_x \rangle = \sqrt{I(I+1)}$ in the angular momentum have been performed. The cranking results for the excitation energies of the 2^+ state are 0.548, 0.591 and 0.571 MeV for ^{34}Mg , ^{32}Mg and ^{30}Mg respectively whereas the corresponding projected quantities are 0.753, 0.873 and 0.895 MeV. The cranking excitation energies of the 2^+ state are a factor 0.7 smaller than the projected ones and therefore, the effect of AMPBV is to increase the moment of inertia as compared to the AMPAV method. If we consider the reduction factor as significative (the q_{20} value chosen roughly corresponds to the position of the maxima of the collective wave functions) and apply it to our GCM results for the $0_1^+ - 2_1^+$ energy differences we obtain the values 0.71, 1.02 and 1.50 MeV for ^{34}Mg , ^{32}Mg and ^{30}Mg respectively. The new energy differences are in much better agreement with the experimental values and the MCSM results than the uncorrected ones. Also the corrected energy obtained for the 4_1^+ state of ^{32}Mg is in good agreement with the excitation energy of 2.3 MeV of a state of this nucleus which is a firm candidate to be the 4^+ state belonging to the Yrast “rotational band” [22]. Although the previous estimation could be criticized in many ways we think it may serve as an indication that a full AMPBV will improve the results obtained here. Concerning the $B(E2)$ transition probabilities, the main effect of the AMPBV will be to shift down the $I = 2, \dots$ projected energy curves keeping its shape mostly unaffected. Therefore, we do not expect big changes both in the collective wave functions $g_\sigma^I(q_{20})$ and in the $B(E)$ transition probabilities that depend on them.

Finally, the band energy diagrams for the three nuclei considered are shown in figure 3 for states with excitation energies smaller than 10 MeV. For each nuclei, the bands labeled (a) and (b) correspond to the GCM result for the

Yrast and excited bands, the band labeled (c) accounts for the experimental data in ^{30}Mg and ^{32}Mg and for the MCSM result in ^{34}Mg and finally, bands (d) and (e) stand for the GCM bands quenched by the factor 0.7 previously discussed.

In conclusion, we have performed angular momentum projected Generator Coordinate Method calculations with the Gogny interaction D1S and the mass quadrupole moment as generating coordinate in order to describe rotational like states in the nuclei ^{30}Mg , ^{32}Mg and ^{34}Mg . We obtain a very well deformed ground state in ^{34}Mg , a fairly deformed ground state in ^{32}Mg and a spherical ground state in ^{30}Mg . In the three nuclei, states with spins higher or equal $I = 4\hbar$ are deformed. The intraband $B(E2)$ transition probabilities agree well with the available experimental data and results from shell model like calculations. The 2^+ excitation energies follow the isotopic trend but come out a factor 1.5 too high as compared with the experiment. We attribute the discrepancy to the well known deficiency of Projection After Variation calculations of providing small moments of inertia. However, we consider the agreement with experiment to be remarkable taking into account that the same force used in this calculation is also able to give reasonable values for such different quantities as fission barrier heights, moments of inertia of superdeformed bands, the energy of octupole vibrations, etc in heavy nuclei.

One of us (R. R.-G.) kindly acknowledges the financial support received from the Spanish Instituto de Cooperacion Iberoamericana (ICI). This work has been supported in part by the DGICyT (Spain) under project PB97/0023.

References

- [1] D. Guillemaud-Müller et al. Nucl. Phys. **A426**, 37 (1984).
- [2] T. Motobayashi et al. Phys. Lett. **B346**, 9 (1995).
- [3] A. Poves and J. Retamosa, Phys. Lett. **B184** (1987) 311; Nucl. Phys. **A571** (1994) 221.
- [4] X. Campi, H. Flocard, A.K. Kerman and S. Koonin, Nucl. Phys. **A251** (1975) 193.
- [5] M. Barranco and R.J. Lombard, Phys. Lett. **B78** (1978) 542.
- [6] R. Bengtsson, P. Möller, J.R. Nix and J. Zhang, Phys. Scr. **29** (1984) 402.
- [7] J. F. Berger et al., Inst. Phys. Conf. Ser. **132** (1993) 487.
- [8] P.-G. Reinhard et al., Phys. Rev. **C60** (1999) 014316.
- [9] R. Rodríguez-Guzmán, J.L. Egido and L.M. Robledo, to appear in Phys. Lett. B, nucl-th/0001003.

- [10] J. Decharge and D. Gogny, Phys. Rev. **C21** (1980) 1568.
- [11] J.F. Berger, M. Girod and D. Gogny, Nucl. Phys. **A428** (1984) 23c.
- [12] P.-H. Heenen, P. Bonche, S. Cwiok, W. Nazarewicz and A. Valor, nucl-th/9908083.
- [13] K. Hara and Y. Sun, Int. J. Mod. Phys. **E4** (1995) 637.
- [14] K. Hara, A. Hayashi and P. Ring, Nucl. Phys. **A385** (1982) 14.
- [15] P. Bonche, J. Dobaczewski, H. Flocard, P. -H. Heenen and J. Meyer, Nucl. Phys. **A510** (1990) 466.
- [16] L. M. Robledo, Phys. Rev. **C50** (1994) 2874; J.L. Egido, L.M. Robledo and Y. Sun, Nucl. Phys. **A560** (1993) 253.
- [17] R. G. Nazmitdinov, L.M. Robledo, P. Ring and J.L. Egido, Nucl. Phys. **A596** (1996) 53.
- [18] A. Valor, J.L. Egido and L.M. Robledo, Phys. Rev. **C53** (1996) 172.
- [19] P. Ring and P. Schuck, *The Nuclear Many Body Problem* (Springer, Berlin, 1980).
- [20] Y. Utsumo, T. Otsuka, T. Mizusaki and M. Honma, Phys. Rev. **C60** (1999) 054315.
- [21] K.W. Schmid and F. Grümmer, Rep. Prog. Phys. **50** (1987) 731.
- [22] F. Azaiez et al., *Proceedings of the Intl. Conf. “Nuclear Structure 98”*, Gatlinburg (1998).
- [23] P.M. Endt, Nucl. Phys. **A521**, (1990) 1.